第 36 卷 第 3 期 原 子 核 物 理 评 论 Vol. 36, No. 3
2019 年 9 月 Nuclear Physics Review Sep., 2019

Article ID: 1007-4627(2019) 03-0357-10

Photoionization of Excited State $3d^{10}4p\ ^2P_{1/2}$ of Cu

GU Sujie[1,2], WAN Jianjie[1,†], GUO Na[1], MA Xinwen[2,†]

(*1. College of Physics and Electronic Engineering, Northwest Normal University, Lanzhou 730070, China;*
2. Institute of Modern Physics, Chinese Academy of Sciences, Lanzhou 730000, China)

Abstract: The calculation of energy level structures is still a challenge for atomic Cu. In the present work, based on the multiconfiguration Dirac-Hartree-Fock (MCDHF) and relativistic configuration interaction (RCI) methods, three large-scale correlation models have been used to calculate the energies and wavefunctions of the singly excited state $3d^{10}4p\ ^2P_{1/2}$, the doubly excited states $3d^94s(^3D)5s\ ^4D_{3/2,1/2}$, $3d^94s(^3D)5s\ ^2D_{3/2}$, $3d^94s(^1D)5s\ ^2D_{3/2}$ and the ionic state $3d^{10}\ ^1S_0$. The results show that the calculated level structures of copper are very sensitive to the choice of finite configuration space. All of the energy differences are less than the existing experimental results by about −0.4 eV between the doubly excited states $3d^94s(^3D)5s\ ^4D_{3/2,1/2}$, $3d^94s(^3D)5s\ ^2D_{3/2}$, $3d^94s(^1D)5s\ ^2D_{3/2}$ and the ionic state $3d^{10}\ ^1S_0$ with the singly excited state $3d^{10}4p\ ^2P_{1/2}$, but the calculated resonant electron energies agree well with the experimental results. In addition, according to the radiative and nonradiative transition matrix elements, the Fano parameters q have been calculated for the doubly excited states. Then, the total photoionization cross sections of singly excited state $3d^{10}4p\ ^2P_{1/2}$ of copper is obtained, where the interference effects can be considered between direct photoionization and photoexcitation autoionization. The resonances $3d^94s(^3D)5s\ ^4D_{3/2,1/2}$, $3d^94s(^3D)5s\ ^2D_{3/2}$, $3d^94s(^1D)5s\ ^2D_{3/2}$ have obvious asymmetrical Fano profiles, which indicates that the interference between photoionization and photoexcitation autoionization has an extremely important influence on the photoionization cross sections near the doubly excited resonances.

Key words: multiconfiguration Dirac-Hartree-Fock (MCDHF) method; singly excited state; doubly excited state; atomic Cu; photoionization cross section

CLC number: O571.6 **Document code:** A **DOI:** 10.11804/NuclPhysRev.36.03.357

1 Introduction

From a fundamental point of view, copper spectroscopy is mainly applied to plasma physics and astrophysics[1]. For example, in various X-ray diffraction experiments[2–3], the copper spectrum is used as a reference light source in the laboratory and an indicator of impurity concentration in high-temperature plasma[4–6]. Copper atoms play an important role in the simulation of copper vapor lasers (CVL)[7–11]. Copper atom has 29 electrons, which like potassium has a big atomic core, however, it has 10 extra electrons in 3d shell, which is the reason why both theoretical and experimental research are widespread[8, 12].

Some theoretical methods were applied to investigate the copper atoms. For instance, Hartree-Fock Slater integrals and semi-empirical Slater parameters for the configurations $3d^94s5s$ and $3d^94s4p$ of Cu have been obtained to describe the structure of this configuration by Wilson[13] within the framework of the JK coupling scheme. Carlsson[14] calculated the energy level and transition probabilities for the singly excited states of Cu by using the multiconfiguration Hartree-Fock (MCHF) approach. Model potential for including correlation effects in relativistic Hartree-Fock (RHF) calculations was proposed by Migdalek and coworkers[15]. A core-polarisation model potential in the RHF approach accounts very well for the discrepancies between uncorrected RHF results and the measured values of the oscillator strengths for the lowest $3d^{10}4s\ ^2S_{1/2}\rightarrow 3d^{10}4p\ ^2P_{1/2,3/2}$ and $3d^{10}4p\ ^2P_{1/2,3/2}\rightarrow 3d^{10}4d\ ^2D_{3/2,5/2}$ transitions in Cu spectra. Msezane and Henry[4] calculated energy levels of $3d^{10}4s\ ^2S$, $3d^94s^2\ ^2D$, $3d^{10}4p\ ^2P$ and $3d^{10}4d\ ^2D$

Received date: 29 Jan. 2019; **Revised date:** 26 Feb. 2019

Foundation item: National Natural Science Foundation of China(11320101003, 11204243); Scientific Research Foundation of Physics of CPEE NWNU

Biography: GU Sujie(1991–), female, Tianshui, Gansu Province, Postgraduate, working on atomic physics; E-mail: gusj0320@163.com

† **Corresponding author:** WAN Jianjie, E-mail: wanjj@nwnu.edu.cn; MA Xinwen, E-mail: x.ma@impcas.ac.cn.

and oscillator strength of $3d^{10}4s\ ^2S\rightarrow 3d^{10}4p\ ^2P$ for Cu with close-coupling method. The target wave function of Cu was constructed to obtain the same oscillator strengths in the dipole length and velocity approximations, which is close to the multiconfiguration Hartree-Fock (MCHF) calculated value by Fischer[16]. Baig and coworkers[17] calculated level structures including wavelengths and effective quantum numbers for the $3d^9 4s6p$ and $3d^9 4s4f$ configurations. Lowe *et al.*[18] have provided the first *ab initio* calculations of shake-off probabilities by finding solutions to relativistic multiconfigurational Dirac-Fock equations accounting for correlation and exchange corrections. In addition to the calculations on the energy structure, Scheibner *et al.*[8] have reported the results of *ab initio* calculations of electron-impact excitation cross sections of atomic copper for the low-lying $3d^{10}4p\ ^2P^o$ and $3d^9 4s^2\ ^2D^e$ excited states. Zatsarinny *et al.*[19] have presented the results from a joint experimental and theoretical investigation of electron impact excitation of the $3d^{10}4s\ ^2S_{1/2}\rightarrow 3d^9 4s^2\ ^2D_{5/2,3/2}$ transitions in copper atoms. Their calculations were performed using nonrelativistic, semirelativistic, and fully relativistic R-matrix (close-coupling) approaches and some oscillator strengths were also deduced. Zatsarinny *et al.*[20] have also used a semirelativistic and a fully relativistic B-spline R-matrix (close-coupling) methods to calculate the elastic electron scattering from the $3d^{10}4s\ ^2S$ ground state and electron-impact excitation of the $3d^{10}4s\ ^2S\rightarrow 3d^{10}4p\ ^2P$ resonance transition in copper atoms. On the other hand, there have also been a lot of experimental studies on copper, such as electron impact excitation[21–22] and ionization[23], resonant Raman scattering[24], photoexcitation and photoionization[25–26], lifetime of exited states[27–29], ionization energy of ground state[30], hyperfine structure[31], Auger spectra[32–35], characteristic spectra[3, 36–37] and so on.

With the development of experimental technology, the photoionization of the singly excited state of copper atom would also be studied. For example, the low-energy photons are used to excite the copper atom from the ground state to the singly excited state $3d^{10}4p\ ^2P_{1/2}$, and then the high-energy photons are used to ionize the copper atom from the singly excited state $3d^{10}4p\ ^2P_{1/2}$. In this paper, the photoionization process of singly excited states is studied theoretically. The dynamic processes include the photoionization processes

$$h\nu + 3d^{10}4p\ ^2P_{1/2} \rightarrow 3d^{10}\ ^1S_0 + \varepsilon s \tag{1}$$

$$h\nu + 3d^{10}4p\ ^2P_{1/2} \rightarrow 3d^{10}\ ^1S_0 + \varepsilon d \tag{2}$$

and the corresponding photoexcitation autoionization processes

$$h\nu + 3d^{10}4p\ ^2P_{1/2} \rightarrow 3d^9 4s(^3D)5s\ ^4D_{1/2} \rightarrow 3d^{10}\ ^1S_0 + \varepsilon s \tag{3}$$

and

$$h\nu + 3d^{10}4p\ ^2P_{1/2} \rightarrow 3d^9 4s(^3D)5s\ ^4D_{3/2} \rightarrow 3d^{10}\ ^1S_0 + \varepsilon d, \tag{4}$$

$$h\nu + 3d^{10}4p\ ^2P_{1/2} \rightarrow 3d^9 4s(^3D)5s\ ^2D_{3/2} \rightarrow 3d^{10}\ ^1S_0 + \varepsilon d, \tag{5}$$

$$h\nu + 3d^{10}4p\ ^2P_{1/2} \rightarrow 3d^9 4s(^1D)5s\ ^2D_{3/2} \rightarrow 3d^{10}\ ^1S_0 + \varepsilon d, \tag{6}$$

where the continuum electrons s and d with the kinetic energy ε are allowed according to the selection rules in the electric dipole approximation. Indeed, the LS coupling scheme is suitable to identify the above atomic states, but the present relativistic calculation is performed based on the jj coupling scheme. Therefore, it is convenient to describe the calculation models in jj coupling scheme but the energy levels are labelled with the LS coupling states so as to avoid ambiguity. In order to study these processes mentioned above, the energies and corresponding wavefunctions of the singly excited state $3d^{10}4p\ ^2P_{1/2}$, the doubly excited states $(3d^9 4s5s)_{J=1/2,3/2}$, and the ionic state $3d^{10}\ ^1S_0$ are calculated with GRASP2K[38] and RATIP[39] code based on the multiconfiguration Dirac-Hartree-Fock (MCDHF) method[40–42] in different large-scale correlation models. Then, the energies and wavefunctions, which are obtained in the most reasonable correlation model, are used to calculate the Fano parameters and (direct) photoionization cross sections. Finally, the photoionization of singly excited state $3d^{10}4p\ ^2P_{1/2}$ of Cu atom is calculated by using the Fano formulism, in which the interference between photoionization and photoexcitation autoionization can be considered with the Fano resonance parameters.

2 Theoretical method

2.1 Multiconfiguration Dirac-Hartree-Fock (MCDHF) and relativistic configuration interaction (RCI) method

In the MCDHF and RCI methods, the state of an atom is represented by atomic state functions (ASFs) $|\Psi(PJM)\rangle$, which are a linear combination of configuration state functions (CSFs) $|\Gamma_r(PJM)\rangle$ with same parity P, total angular momentum J and its z direction component M.

$$|\Psi(PJM)\rangle = \sum_{r=1}^{n_c} C_r^{\Psi}\, |\Gamma_r(PJM)\rangle\,, \tag{7}$$

where n_c is the number of CSFs and the CSF $|\Gamma_r(PJM)\rangle$ is antisymmetrized linear combinations of

Slater determinant formed with one-electron spin orbitals,

$$\psi_{n\kappa m}(\vec{r}) = \frac{1}{r}\begin{pmatrix} P_{n\kappa}(r)\chi_{\kappa m}(\theta,\phi) \\ iQ_{n\kappa}(r)\chi_{-\kappa m}(\theta,\phi) \end{pmatrix}, \tag{8}$$

where n is principal quantum number and κ is called as relativistic angular quantum number, $P_{n\kappa}(r)$ and $Q_{n\kappa}(r)$ are the large and small components of radial wavefunctions, and $\chi_{\kappa m}(\theta,\phi)$ is the spinor spherical harmonic function.

In the present calculations, the (transverse) Breit interaction is also added by diagonalizing the Dirac-Coulomb-Breit Hamiltonian matrix. The nucleus finite size and motion effects are also considered. In addition, the dominant quantum electrodynamic (QED) contribution, *i.e.* self-energy and vacuum polarization effects, are also included in the computation of the energies in the hydrogen-like approximation and as perturbation.

2.2 Photoionization cross section

The interference effect of isolated resonance on the total photoionization cross section was derived originally by Fano and coworkers[43–44]. The expression for the total cross section $\sigma(\omega)$ for a photon of energy ω in the case of a singly discrete state interacting with one or more continuum states is as follows:

$$\sigma(\omega) = \sigma_{if}^{PI}(\omega)\left(\rho_{ijf}^2\frac{(q_{ijf}+\widetilde{\omega})^2}{1+\widetilde{\omega}^2} + 1 - \rho_{ijf}^2\right), \tag{9}$$

where $\sigma_{if}^{PI}(\omega)$ is the direct photoionization cross section from initial ionic state i to final ionic state f, the Fano parameter q, which governs the (interference) shape of the cross section, is given by

$$q_{ijf} = \frac{\langle\Phi_j\|O^{(L)}\|\Psi_i\rangle}{\pi\sum\limits_{\kappa}\langle\Psi_j\|\sum\limits_{p<q}V_{pq}\|\Psi_f,\varepsilon\kappa;\Psi_{f\prime}\rangle\langle\Psi_f,\varepsilon\kappa;\Psi_{f\prime}\|O^{(L)}\|\Psi_i\rangle} \tag{10}$$

and the correlation coefficient ρ^2, which is a measure of the strength of the resonance, is defined as

$$\rho_{ijf}^2 = \frac{[\sum\limits_{\kappa}\langle\Psi_j\|\sum\limits_{p<q}V_{pq}\|\Psi_f,\varepsilon\kappa;\Psi_{f\prime}\rangle\langle\Psi_f,\varepsilon\kappa;\Psi_{f\prime}\|O^{(L)}\|\Psi_i\rangle]^2}{[\sum\limits_{\kappa}(\langle\Psi_j\|\sum\limits_{p<q}V_{pq}\|\Psi_f,\varepsilon\kappa;\Psi_{f\prime}\rangle)^2][\sum\limits_{\kappa}(\langle\Psi_f,\varepsilon\kappa;\Psi_{f\prime}\|O^{(L)}\|\Psi_i\rangle)^2]}, \tag{11}$$

and

$$\widetilde{\omega} = \frac{\omega - E_r}{\Gamma/2} = \frac{\omega - E_{ji} - \Delta_r}{\Gamma/2}, \tag{12}$$

describes the departure of the incident photon energy ω from a resonance center $E_r = E_{ji} + \Delta_r$, where $E_{ji} = E_j - E_i$ the resonance energy between initial state i and resonant state j and the quantity Δ_r represents thus a shift of the resonance center with respect to E_{ji}. The shift is usually regarded as approximately zero in practical calculations so that the resonance center is given only by E_{ji}. Γ is line width of resonance, which is considered as a sum of Auger and radiative widths, but for neutral atom, the radiative widths are rather less than Auger width, so the line width is assumed to be the Auger width given by

$$\Gamma^{\text{auger}} = 2\pi\sum_{\kappa}|\langle\Psi_f,\varepsilon\kappa;\Psi_{f\prime}|\sum_{p<q}V_{pq}|\Psi_j\rangle|^2 \tag{13}$$

where Ψ_j is the atomic state function of the autoionization state j, $\Psi_{f\prime}$ is the atomic state function of the system formed by ionic state Ψ_f and a continuum electron κ with energy ε. The two-electron operator V_{pq} in the expression (10), (11) and (13) is the sum of Coulomb and Breit operators, which has the form in atomic units

$$V_{pq} = \frac{1}{r_{pq}} - \alpha_p.\alpha_q\frac{\cos(\omega_{pq}r_{pq})}{r_{pq}} + (\alpha_p.\nabla_p)(\alpha_q.\nabla_q)\frac{\cos(\omega_{pq}r_{pq})-1}{\omega_{pq}^2 r_{pq}}, \tag{14}$$

where α_p and α_q are Dirac vector matrixes. and ω_{pq} is the wave number of the exchange virtual photon, and the Auger rate A_{jf}^a is equal to the Auger linewidth in atomic units. The calculation of all the parameters can refer to our previous work[45].

In the present work, the photoionization

$$h\nu + 3d^{10}4p_{1/2}\ ^2P_{1/2} \to 3d^{10}\ ^1S_0 + \varepsilon s_{1/2} \tag{15}$$

and its corresponding photoexcitation autoionization

$$h\nu + 3d^{10}4p_{1/2}\ ^2P_{1/2} \to [(3d_{3/2}^3 3d_{5/2}^6 4s_{1/2})_1 5s_{1/2}]_{1/2} \to 3d^{10}\ ^1S_0 + \varepsilon s_{1/2} \tag{16}$$

are just this case. Both of the two processes mentioned above have only one continuum electron $s_{1/2}$ and the total cross section can be simplified as

$$\sigma(\omega) = \sigma_{if}^{PI}(\omega)\frac{(q_{ijf}+\widetilde{\omega})^2}{1+\widetilde{\omega}^2}, \tag{17}$$

because

$$\rho^2 = 1. \tag{18}$$

In addition to the above case, Fano[44] also proposed another case in which there are a number of discrete states and one continuum state. In this work, the following processes are considered

$$h\nu + 3d^{10}4p_{1/2}\ {}^2P_{1/2} \to 3d^{10}\ {}^1S_0 + \varepsilon d_{3/2}, \tag{19}$$

$$\begin{aligned} h\nu + 3d^{10}4p_{1/2}\ {}^2P_{1/2} &\to [(3d^4_{3/2}3d^5_{5/2}4s_{1/2})_2 5s_{1/2}]_{3/2} \\ &\to 3d^{10}\ {}^1S_0 + \varepsilon d_{3/2}, \end{aligned} \tag{20}$$

$$\begin{aligned} h\nu + 3d^{10}4p_{1/2}\ {}^2P_{1/2} &\to [(3d^3_{3/2}3d^6_{5/2}4s_{1/2})_1 5s_{1/2}]_{3/2} \\ &\to 3d^{10}\ {}^1S_0 + \varepsilon d_{3/2}, \end{aligned} \tag{21}$$

$$\begin{aligned} h\nu + 3d^{10}4p_{1/2}\ {}^2P_{1/2} &\to [(3d^3_{3/2}3d^6_{5/2}4s_{1/2})_2 5s_{1/2}]_{3/2} \\ &\to 3d^{10}\ {}^1S_0 + \varepsilon d_{3/2}, \end{aligned} \tag{22}$$

which includes three discrete states and one continuum state $d_{3/2}$, so the total cross section is given by

$$\sigma(\omega) = \sigma^{PI}_{if}(\omega)\frac{1}{1+(\sum\limits_j \frac{1}{\widetilde{\omega}_j})^2}\Big(\sum_j \frac{q_{ijf}}{\widetilde{\omega}_j} + 1\Big)^2 \tag{23}$$

where $\widetilde{\omega}_j$ is reduced energy relative to the j_{th} resonance similar to $\widetilde{\omega}$.

3 Results and discussion

As is known, the charge density of residual electrons will be rearranged due to the changed potential in radiative and nonradiative processes and this is called orbital relaxation. As far as we know, orbital relaxation is a general phenomenon in various dynamical processes, especially for neutral atoms and lowly charged ions. As for the multielectron atoms, the electron orbitals of Cu can redistribute during transition processes such as excitation, ionization, radiative and Auger transition and so on. To demonstrate the effects, the wave functions for the initial state $3d^{10}4p\ {}^2P_{1/2}$, final ionic state $3d^{10}\ {}^1S_0$ and doubly excited states $(3d^9 4s5s)_{J=1/2,3/2}$ have been calculated separately in single configuration (SC) approximation. Table 1 gives the mean radii of occupied $1s$, $2s$, $2p_{1/2}$, $2p_{3/2}$, $3s$, $3p_{1/2}$, $3p_{3/2}$, $3d_{3/2}$, $3d_{5/2}$, $4s$, $4p_{1/2}$, $5s$ orbitals in the singly excited state $3d^{10}4p\ {}^2P_{1/2}$, the doubly excited states $(3d^9 4s5s)_{J=1/2,3/2}$, and the ionic state $3d^{10}\ {}^1S_0$.

As can be seen from Table 1, the mean radii of the radial orbitals with $n = 1$ and 2 are nearly the same for either the initial ionic state $3d^{10}4p_{1/2}\ {}^2P_{1/2}$, the final ionic state $3d^{10}\ {}^1S_0$ or the doubly excited states $(3d^9 4s5s)_{J=1/2,3/2}$. This shows that the relaxation of the orbitals with $n = 1$ and 2 is very weak in the processes of photoionization and photoexcitation autoionization. In the photoionization, only the $3d$ orbitals changed slightly larger in the initial $3d^{10}4p_{1/2}\ {}^2P_{1/2}$ and final $3d^{10}\ {}^1S_0$ ionic states, which illustrates the ionization of $4p_{1/2}$ electron has the biggest influence on the electrons in outmost shells *i.e.* $3d_{3/2}$ and $3d_{5/2}$ electron. What's interesting is that, during the photoexcitation autoionization process, the mean radii of the orbitals with $n = 3$ firstly decreases and then increases with significant changes.

Table 1 Mean radii of occupied orbitals.

Orbitals	States		
	$3d^{10}4p_{1/2}\ {}^2P_{1/2}$	$(3d^9 4s5s)_{J=1/2,3/2}$	$3d^{10}\ {}^1S_0$
$1s$	5.23E-02	5.21E-02	5.22E-02
$2s$	2.35E-01	2.35E-01	2.34E-01
$2p_{1/2}$	2.05E-01	2.05E-01	2.04E-01
$2p_{3/2}$	2.08E-01	2.08E-01	2.07E-01
$3s$	7.12E-01	7.08E-01	7.13E-01
$3p_{1/2}$	7.45E-01	7.39E-01	7.47E-01
$3p_{3/2}$	7.55E-01	7.49E-01	7.57E-01
$3d_{3/2}$	9.85E-01	9.14E-01	9.77E-01
$3d_{5/2}$	9.89E-01	9.20E-01	9.87E-01
$4s$	-	2.67E+00	-
$4p_{1/2}$	5.10E+00	-	-
$5s$	-	8.59E+00	-

In addition to the electron relaxation, electron correlation also plays a crucial role in atomic structure for neutral atoms and low charge low-Z ions. In the framework of MCDHF method, electron correlation can be considered by increasing the CSFs with the same symmetry. In order to include a sufficiently large number of CSFs, the active space method as discussed by Roos *et al.*[46] is used to generate the CSFs systematically. Therefore, a complete relaxed MCDHF calculation in the extensive optimized level (EOL) scheme is implemented in the present work. To investigate the effect of the size of wavefunctions on excitation/ionization energy and transition properties, a series of large-scale MCDHF and RCI computations are carried out for the selected levels and transitions between those levels by enlarging the configuration spaces in different correlation models. In general, in model C_1 all the orbitals $1s, 2s, 2p, 3s, 3p, 3d$ are active. In model C_2 inactive core orbitals and active orbitals are chosen as $1s$ and $2s, 2p, 3s, 3p, 3d$, respectively. In model C_3, $1s, 2s, 2p$ subshells are regarded as inactive core orbitals and $3s, 3p, 3d$ are treated as active orbitals. In the three models, the electron correlation can be considered by allowing single and double (SD) substitution within the active set of orbitals, which is enlarged at each

step of calculation, and then the existing optimized orbitals are frozen after each expansion. SD substitutions from active orbitals into virtual orbitals with n=4, 5, 6, 7 produces configuration spaces: 4SD, 5SD, 6SD and 7SD. Apart from the SC configuration space, all virtual single (S) and double (D) excitations from the occupied shells into the unoccupied shells are taken into account. For simplicity, the relativistic angular momentum is omitted here except for $4p_{3/2}$. Definitely, for the initial state $3d^{10}4p_{1/2}\ ^2P_{1/2}$, the unoccupied subshells include $\{4s,4p_{3/2},4d,4f\}$, $\{5s,5p,5d,5f,5g\}$, $\{6s,6p,6d,6f,6g,6h\}$ and $\{7s,7p,7d,7f,7g,7h,7i\}$. For the doubly excited states $(3d^9 4s5s)_{J=1/2,3/2}$, the virtual subshells include $\{4p,4d,4f\}$, $\{5p,5d,5f,5g\}$, $\{6s,6p,6d,6f,6g,6h\}$ and $\{7s,7p,7d,7f,7g,7h,7i\}$. For the ionized state $3d^{10}\ ^1S_0$, the virtual subshells include $\{4s,4p,4d,4f\}$, $\{5s,5p,5d,5f,5g\}$, $\{6s,6p,6d,6f,6g,6h\}$ and $\{7s,7p,7d,7f,7g,7h,7i\}$. For the sake of brevity, these configuration spaces are denoted by 4SD, 5SD, 6SD and 7SD, respectively. For example, 5SD represents the excitation to $\{4s,4p_{3/2},4d,4f\}$ and $\{5s,5p,5d,5f,5g\}$ for the initial state $3d^{10}4p_{1/2}\ ^2P_{1/2}$ and excitation to $\{4p,4d,4f\}$ and $\{5p,5d,5f,5g\}$ for the doubly excited states $(3d^9 4s5s)_{J=1/2,3/2}$. For the ionized state $3d^{10}\ ^1S_0$, 5SD represents the excitation to $\{4s,4p,4d,4f\}$ and $\{5s,5p,5d,5f,5g\}$.

Tables 2, 3 and 4 show the number of CSFs in different correlation models, which are utilized in the wavefunction expansion with a given total angular momentum and parity J^P. From the tables, it is apparent to find that the number of CSFs is increased rapidly with enlarging the configuration space and the more active orbitals the more CSFs. The maximum number of 1586366 CSFs appears in 7SD configuration space in model C_1, which reaches to the limit of present calculation. Tables 5, 6 and 7 present the eigenvalues for three correlation models, although the convergent energy differences are focused on instead of the eigenvalues for multielectron atoms like Cu. With the enlargement of configuration spaces, the eigenvalues become more and more negative and convergent, as satisfies the requirement of variational principle.

Table 2　Configuration space and number of CSFs in model C_3.

Configuration space	States			
	$3d^{10}4p_{1/2}\ ^2P_{1/2}$	$3d^{10}\ ^1S_0$	$(3d^9 4s5s)_{3/2}$	$(3d^9 4s5s)_{1/2}$
SC	1	1	3	1
4SD	2 127	306	15 350	8 724
5SD	12 929	1 442	78 895	44 363
6SD	37 148	3 872	235 931	129 401
7SD	79 053	7 659	514 814	278 803

Table 3　Configuration space and number of CSFs in model C_2.

Configuration space	States			
	$3d^{10}4p_{1/2}\ ^2P_{1/2}$	$3d^{10}\ ^1S_0$	$(3d^9 4s5s)_{3/2}$	$(3d^9 4s5s)_{1/2}$
SC	1	1	3	1
4SD	4 772	678	39 615	22 551
5SD	28 779	3214	205 341	114 427
6SD	82 019	8 385	606 608	333 024
7SD	173 395	16 891	1 321 105	714 028

Table 4　Configuration space and number of CSFs in model C_1.

Configuration space	States			
	$3d^{10}4p_{1/2}\ ^2P_{1/2}$	$3d^{10}\ ^1S_0$	$(3d^9 4s5s)_{3/2}$	$(3d^9 4s5s)_{1/2}$
SC	1	1	3	1
4SD	5 659	806	47 952	27 330
5SD	34 044	3 811	248 229	138 435
6SD	96 754	9 914	729 105	400 489
7SD	204 087	19 924	1 586 366	860 066

Table 5　Eigenvalues in a.u. of the singly excited state $3d^{10}4p_{1/2}\ ^2P_{1/2}$, the doubly excited state $(3d^9 4s5s)_{J=1/2,3/2}$, and the ionic state $3d^{10}\ ^1S_0$ in model C_3.

Configuration space	States					
	$3d^{10}4p_{1/2}\ ^2P_{1/2}$	$3d^{10}\ ^1S_0$	$3d^9 4s(^3D)5s\ ^4D_{3/2}$	$3d^9 4s(^3D)5s\ ^4D_{1/2}$	$3d^9 4s(^3D)5s\ ^2D_{3/2}$	$3d^9 4s(^1D)5s\ ^2D_{3/2}$
SC	−1652.7370	−1652.6126	−1652.6722	−1652.6684	−1652.6633	−1652.6461
4SD	−1653.2495	−1653.1767	−1653.1438	−1653.1398	−1653.1364	−1653.1229
5SD	−1653.4828	−1653.3634	−1653.3112	−1653.3073	−1653.3038	−1653.2909
6SD	−1653.5720	−1653.4453	−1653.4351	−1653.4323	−1653.4279	−1653.4163
7SD	−1653.6098	−1653.4804	−1653.4739	−1653.4700	−1653.4668	−1653.4551

Table 6 Eigenvalues in a.u. of the singly excited state $3d^{10}4p_{1/2}\ ^2P_{1/2}$, the doubly excited state $(3d^9 4s5s)_{J=1/2,3/2}$, and the ionic state $3d^{10}\ ^1S_0$ in model C_2.

Configuration space	States					
	$3d^{10}4p_{1/2}\ ^2P_{1/2}$	$3d^{10}\ ^1S_0$	$3d^9 4s(^3D)5s\ ^4D_{3/2}$	$3d^9 4s(^3D)5s\ ^4D_{1/2}$	$3d^9 4s(^3D)5s\ ^2D_{3/2}$	$3d^9 4s(^1D)5s\ ^2D_{3/2}$
SC	−1652.7370	−1652.6126	−1652.6722	−1652.6684	−1652.6633	−1652.6461
4SD	−1653.2741	−1653.2075	−1653.1721	−1653.1677	−1653.1656	−1653.1532
5SD	−1653.6822	−1653.5910	−1653.5049	−1653.5007	−1653.4979	−1653.4850
6SD	−1653.8783	−1653.7593	−1653.7092	−1653.7035	−1653.7019	−1653.6897
7SD	−1653.9694	−1653.8451	−1653.8325	−1653.8230	−1653.8251	−1653.8129

Table 7 Eigenvalues in a.u. of the singly excited state $3d^{10}4p_{1/2}\ ^2P_{1/2}$, the doubly excited state $(3d^9 4s5s)_{J=1/2,3/2}$, and the ionic state $3d^{10}\ ^1S_0$ in model C_1.

Configuration space	States					
	$3d^{10}4p_{1/2}\ ^2P_{1/2}$	$3d^{10}\ ^1S_0$	$3d^9 4s(^3D)5s\ ^4D_{3/2}$	$3d^9 4s(^3D)5s\ ^4D_{1/2}$	$3d^9 4s(^3D)5s\ ^2D_{3/2}$	$3d^9 4s(^1D)5s\ ^2D_{3/2}$
SC	−1652.7370	−1652.6126	−1652.6722	−1652.6684	−1652.6633	−1652.6461
4SD	−1653.2742	−1653.2078	−1653.1722	−1653.1678	−1653.1657	−1653.1533
5SD	−1653.6947	−1653.6087	−1653.5112	−1653.5064	−1653.5040	−1653.4912
6SD	−1653.9175	−1653.8038	−1653.7267	−1653.7206	−1653.7193	−1653.7070
7SD	−1654.0279	−1653.9070	−1653.8646	−1653.8591	−1653.8572	−1653.8449

Tables 8, 9 and 10 give energy levels related to the initial state $3d^{10}4p_{1/2}\ ^2P_{1/2}$ in different configuration spaces. In these tables, the ionization energy is reasonable, but the calculated energies of the doubly excited states are lower than that of the ionized state. Therefore only a very rough estimate of the ionization energy is given in the SC approximation. Among the three correlation models, the most convergent results have been obtained in model C_3 with the increase of the CSFs. In Figs. 1∼3, the convergent behavior can be shown apparently in model C_3, and the fine structures are also reasonable with comparison to the experiment although all of the energies of the doubly excited states and the ionic sate have a shift from NIST[47] by around 0.4 eV. It is obvious for Cu that energy differences are very sensitive to the correlation models and the calculated results are very unsatisfactory in models C_1 and C_2.

Table 8 Energy level in eV related to the initial state $3d^{10}4p_{1/2}\ ^2P_{1/2}$ in model C_3.

States	Configuration space					
	SC	4SD	5SD	6SD	7SD	NIST[47]
$3d^{10}4p_{1/2}\ ^2P_{1/2}$	0.000 0	0.000 0	0.000 0	0.000 0	0.000 0	0.000 0
$3d^{10}\ ^1S_0$	3.385 9	1.980 9	3.248 3	3.446 4	3.519 7	3.940 5
$3d^9 4s(^3D)5s\ ^4D_{3/2}$	1.764 3	2.875 1	4.667 9	3.726 5	3.697 4	4.097 6
$3d^9 4s(^3D)5s\ ^4D_{1/2}$	1.866 9	2.985 2	4.774 5	3.802 5	3.803 3	4.207 7
$3d^9 4s(^3D)5s\ ^2D_{3/2}$	2.006 0	3.078 0	4.870 4	3.919 9	3.890 4	4.305 3
$3d^9 4s(^1D)5s\ ^2D_{3/2}$	2.475 0	3.444 2	5.219 9	4.237 7	4.207 1	4.641 6

Table 9 Energy level in eV related to the initial state $3d^{10}4p_{1/2}\ ^2P_{1/2}$ in model C_2.

States	Configuration space					
	SC	4SD	5SD	6SD	7SD	NIST[47]
$3d^{10}4p_{1/2}\ ^2P_{1/2}$	0.000 0	0.000 0	0.000 0	0.000 0	0.000 0	0.000 0
$3d^{10}\ ^1S_0$	3.385 9	1.810 8	2.479 9	3.235 7	3.383 4	3.940 5
$3d^9 4s(^3D)5s\ ^4D_{3/2}$	1.764 3	2.776 0	4.823 4	4.599 5	3.725 7	4.097 6
$3d^9 4s(^3D)5s\ ^4D_{1/2}$	1.866 9	2.893 9	4.937 2	4.756 3	3.984 8	4.207 7
$3d^9 4s(^3D)5s\ ^2D_{3/2}$	2.006 0	2.951 8	5.015 5	4.798 1	3.926 6	4.305 3
$3d^9 4s(^1D)5s\ ^2D_{3/2}$	2.475 0	3.288 2	5.364 4	5.130 1	4.258 8	4.641 6

Table 10　Energy level in eV related to the initial state $3d^{10}4p_{1/2}\ ^2P_{1/2}$ in model C_1.

States	Configuration space					
	SC	4SD	5SD	6SD	7SD	NIST[47]
$3d^{10}4p_{1/2}\ ^2P_{1/2}$	0.000 0	0.000 0	0.000 0	0.000 0	0.000 0	0.000 0
$3d^{10}\ ^1S_0$	3.385 9	1.808 0	2.341 6	3.092 9	3.290 0	3.940 5
$3d^9 4s(^3D)5s\ ^4D_{3/2}$	1.764 3	2.777 0	4.994 1	5.191 9	4.443 4	4.097 6
$3d^9 4s(^3D)5s\ ^4D_{1/2}$	1.866 9	2.895 0	5.124 8	5.357 4	4.592 4	4.207 7
$3d^9 4s(^3D)5s\ ^2D_{3/2}$	2.006 0	2.953 0	5.189 5	5.392 8	4.645 1	4.305 3
$3d^9 4s(^1D)5s\ ^2D_{3/2}$	2.475 0	3.289 6	5.537 2	5.727 6	4.978 6	4.641 6

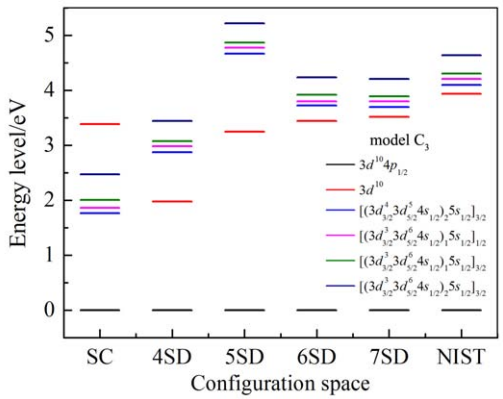

Fig. 1　(color online) Energy level related to the initial state $3d^{10}4p_{1/2}\ ^2P_{1/2}$ in model C_3.

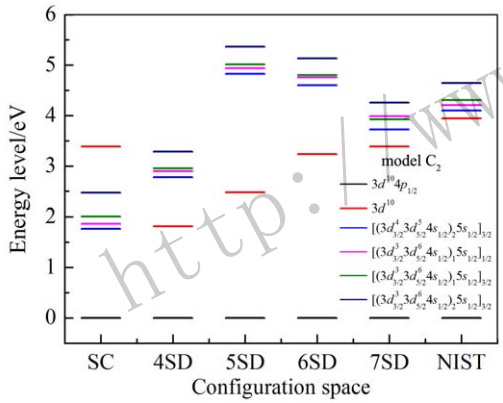

Fig. 2　(color online) Energy level related to the initial state $3d^{10}4p_{1/2}\ ^2P_{1/2}$ in model C_2.

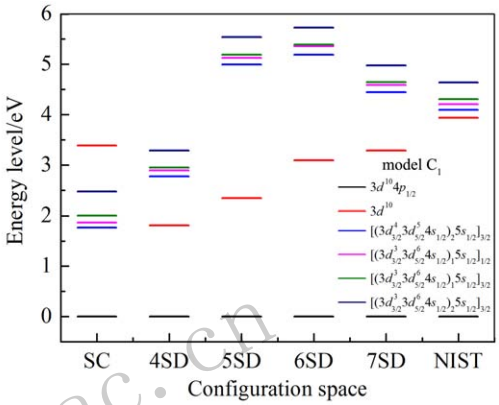

Fig. 3　(color online) Energy level related to the initial state $3d^{10}4p_{1/2}\ ^2P_{1/2}$ in model C_1.

The same situation happens to the resonance electron energy from Tables 11∼13. The calculation is very rough in SC approximation, because the energy is lower than the ionization energy and both of the resonance electron energies are unreasonable in models C_1 and C_2 with increasing the number of CSFs. However, when the configuration space reaches to 7SD in model C_3, the resonance energies can be acceptable for the doubly excited states.

Based on the energies and wavefunctions given in model C_3, the resonance parameters are calculated, including the Fano parameters q and Auger widths, as given in Table 14, then the photoionization cross sec-

Table 11　Resonant electron energy in eV for the intermediate states in model C_3.

Doubly excited states	Configuration space					
	SC	4SD	5SD	6SD	7SD	NIST[47]
$3d^9 4s(^3D)5s\ ^4D_{3/2}$	−1.621 6	0.894 3	1.419 6	0.280 1	0.177 7	0.157 1
$3d^9 4s(^3D)5s\ ^4D_{1/2}$	−1.519 0	1.004 4	1.526 1	0.356 2	0.283 6	0.267 2
$3d^9 4s(^3D)5s\ ^2D_{3/2}$	−1.379 8	1.097 2	1.622 1	0.473 6	0.370 8	0.364 8
$3d^9 4s(^1D)5s\ ^2D_{3/2}$	−0.910 9	1.463 4	1.971 6	0.791 3	0.687 5	0.701 1

Table 12　Resonant electron energy in eV for the intermediate states in model C_2.

Doubly excited states	Configuration space					
	SC	4SD	5SD	6SD	7SD	NIST[47]
$3d^9 4s(^3D)5s\ ^4D_{3/2}$	−1.621 6	0.965 2	2.343 5	1.363 8	0.342 4	0.157 1
$3d^9 4s(^3D)5s\ ^4D_{1/2}$	−1.519 0	1.083 1	2.457 2	1.520 6	0.601 4	0.267 2
$3d^9 4s(^3D)5s\ ^2D_{3/2}$	−1.379 8	1.141 0	2.535 6	1.562 4	0.543 3	0.364 8
$3d^9 4s(^1D)5s\ ^2D_{3/2}$	−0.910 9	1.477 4	2.884 4	1.894 4	0.875 5	0.701 1

Table 13 Resonant electron energy in eV for the intermediate states in model C_1.

Doubly excited states	Configuration space					
	SC	4SD	5SD	6SD	7SD	NIST[47]
$3d^9 4s(^3D)5s\ ^4D_{3/2}$	−1.621 6	0.969 0	2.652 6	2.099 0	1.153 3	0.157 1
$3d^9 4s(^3D)5s\ ^4D_{1/2}$	−1.519 0	1.087 0	2.783 3	2.264 5	1.302 4	0.267 2
$3d^9 4s(^3D)5s\ ^2D_{3/2}$	−1.379 8	1.145 0	2.847 9	2.300 0	1.355 1	0.364 8
$3d^9 4s(^1D)5s\ ^2D_{3/2}$	−0.910 9	1.481 6	3.195 6	2.634 8	1.688 6	0.701 1

Table 14 Auger width Γ and Fano parameters q for the doubly excited states.

Doubly excited states	Γ/meV	q_{ijf}
$3d^9 4s(^3D)5s\ ^4D_{3/2}$	1.01E-01	−0.73
$3d^9 4s(^3D)5s\ ^4D_{1/2}$	3.92E-07	827.82
$3d^9 4s(^3D)5s\ ^2D_{3/2}$	1.14E-02	−5.67
$3d^9 4s(^1D)5s\ ^2D_{3/2}$	4.74E+00	−0.21

tions have been calculated involving the doubly excited resonances $3d^9 4s(^3D)5s\ ^4D_{3/2,1/2}$, $3d^9 4s(^3D)5s\ ^2D_{3/2}$, $3d^9 4s(^1D)5s\ ^2D_{3/2}$. The values of the Fano parameters q are negative for the resonances $3d^9 4s(^3D)5s\ ^4D_{3/2}$, $3d^9 4s(^3D)5s\ ^2D_{3/2}$ and $3d^9 4s(^1D)5s\ ^2D_{3/2}$, while the value of q is positive for the resonance $3d^9 4s(^3D)5s\ ^4D_{1/2}$. Therefore, the photoionization cross sections show asymmetrical Fano profiles in Fig. 4. Furthermore, the resonance $3d^9 4s(^1D)5s\ ^2D_{3/2}$ gives the so-called window resonance because the value of q closes to zero, the shape of which would be obvious when the width is large.

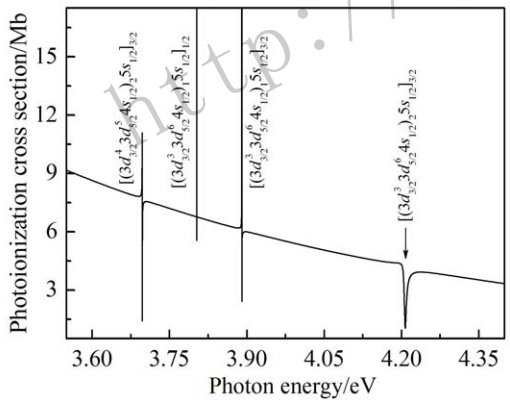

Fig. 4 (color online) Photoionization cross sections of singly excited state $3d^{10}4p_{1/2}\ ^2P_{1/2}$ involving the doubly excited states $3d^9 4s(^3D)5s\ ^4D_{3/2,1/2}$, $3d^9 4s(^3D)5s\ ^2D_{3/2}$, $3d^9 4s(^1D)5s\ ^2D_{3/2}$.

4 Conclusions

In the present work, relaxed orbitals have been optimized in the states with different J^P, because it is well known that the electron distribution would be changed drastically when a lowly-ionized ion absorb/emits a photon or an electron especially for neutral atom. On the other hand, in order to describe the atomic states, within the framework of MCDHF and RCI methods, the energies and wavefunctions of the singly excited state $3d^{10}4p\ ^2P_{1/2}$, the doubly excited states $3d^9 4s(^3D)5s\ ^4D_{3/2,1/2}$, $3d^9 4s(^3D)5s\ ^2D_{3/2}$, $3d^9 4s(^1D)5s\ ^2D_{3/2}$ and the ionic state $3d^{10}\ ^1S_0$ were calculated by systematically enlarging the configuration space. As we know, it is extremely difficult to calculate the energies of neutral atoms, especially for their doubly excited states. Three correlation models have been used to describe the singly excited state $3d^{10}4p\ ^2P_{1/2}$, the doubly excited states $3d^9 4s(^3D)5s\ ^4D_{3/2,1/2}$, $3d^9 4s(^3D)5s\ ^2D_{3/2}$, $3d^9 4s(^1D)5s\ ^2D_{3/2}$ and the ionic state $3d^{10}\ ^1S_0$. The eigenvalues are more and more negative with the increase of the number of CSFs indeed. According to the present calculation, however, it is found that the calculated energies from the model C_3 are closest to the experimental results with comparison to the other models. It means that for Cu the energy differences between the different energy levels are very sensitive to the finite configuration space.

On the basis of the wavefunctions and energies from model C_3, the resonance parameters including the resonance electron energies, Auger widths and Fano parameters q have been calculated and then the photoionization cross sections have been obtained involving the doubly excited resonances from the singly excited state $3d^{10}4p\ ^2P_{1/2}$ of the copper atom. The results show that the interference between photoionization and photoexcitation autoionization processes has a very important influence on the photoionization cross sections around the doubly excited resonances $3d^9 4s(^3D)5s\ ^4D_{3/2,1/2}$, $3d^9 4s(^3D)5s\ ^2D_{3/2}$, $3d^9 4s(^1D)5s\ ^2D_{3/2}$, that is, the photoionization cross sections show asymmetrical Fano profiles around the resonances $3d^9 4s(^3D)5s\ ^4D_{3/2,1/2}$, $3d^9 4s(^3D)5s\ ^2D_{3/2}$ and $3d^9 4s(^1D)5s\ ^2D_{3/2}$, especially there is a window resonance at $3d^9 4s(^1D)5s\ ^2D_{3/2}$. Of course, it is expected that a more reasonable correlation model will be tried to obtain more accurate wave functions and energy levels in our next work.

References:

[1] CHANTLER C T, LOWE J A, GRANT I P. Phys Rev A, 2010, **82**: 052505.

[2] HINNOV E, SUCKEWER S, COHEN S, SATO K. Phys Rev A, 1982, **25**: 2293-2301.
[3] DEUTSCH M, HÖLZER G, HÄRTWIGS J, *et al*. Phys Rev A, 1995, **51**: 283.
[4] MSEZANE A Z, HENRY R J W. Phys Rev A, 1986, **33**: 1631.
[5] CHANTLER C T, HAYWARD A C L, GRANT I P. Phys Rev Lett, 2009, **103**: 123002.
[6] CHANTLER C T, LOWE J A, GRANT I P. Phys Rev A, 2012, **85**: 032513.
[7] WILLIAMS W, TRAJMAR S. Phys Rev Lett, 1974, **33**: 187.
[8] SCHEIBNER K F, HAZI A U, HENRY R J W. Phys Rev A, 1987, **35**: 4869.
[9] ZHANG J Y, MITROY J, SADEGHPOUR H R, *et al*. Phys Rev A, 2008, **78**: 062710.
[10] ZATSARINNY O, BARTSCHAT K, SUVOROV V, *et al*. Phys Rev A, 2010, **81**: 062705.
[11] ZATSARINNY O, BARTSCHAT K. Phys Rev A, 2010, **82**: 062703.
[12] CURTIS L J, THEODOSIOU C E. Phys Rev A, 1989, **39**: 605.
[13] WILSON M. J Phys B, 1969, **2**: 524.
[14] CARLSSON J. Phys Rev A, 1988, **38**: 1702.
[15] MIGDALEK J, BAYLIS W E. J Phys B, 1978, **11**: L497.
[16] FISCHER C F. J Phys B. 1977, **10**: 1241.
[17] BAIG M A, RASHID A, HANIF M, *et al*. Phys Rev A, 1992, **45**: 2108.
[18] LOWE J A, CHANTLER C T, GRANT I P. Phys Rev A, 2011, **83**: 060501.
[19] ZATSARINNY O, BARTSCHAT K, SUVOROV V, *et al*. Phys Rev A, 2010, **81**: 062705.
[20] ZATSARINNY O, BARTSCHAT K. Phys Rev A, 2010, **82**: 062703.
[21] TRAJMAR S, WILLIAMS W, SRIVASTAVA S K. J Phys B, 1977, **10**: 3323.
[22] WILLIAMS W, TRAJMAR S. Phys Rev Lett, 1974, **33**: 187.
[23] LLOVET X, MERLET C, SALVAT F. J Phys B, 2000, **33**: 3761.
[24] SÁNCHEZ H J, VALENTINUZZI M C, PÉREZ C. J Phys B, 2006, **39**: 4317.
[25] MURTY V R K, RAO K S, PARTHASARADHI K, *et al*. J Phys B, 1977, **10**: 3189.
[26] NATHURAM R, SUNDARA RAO I S, MEHTA M K. Phys Rev A, 1988, **37**: 4978.
[27] KRELLMANN H, SIEFART E, WEIHRETER E. J Phys B, 1975, **8**: 2608.
[28] SIEFART E, NEY J, BUCKA H, *et al*. J Phys B, 1974, **7**: 1279.
[29] ZERNE R, LARSSON J, SVANBERG S. Phys Rev A, 1994, **49**: 128.
[30] LOOCK HANS-PETER, BEATY LEANNE M, SIMARD BENOIT. Phys Rev A, 1999, **59**: 873.
[31] BENGTSSON J, LARSSON J, SVANBERG S, *et al*. Phys Rev A, 1990, **41**: 233.
[32] TERRENCE J, POWELL C J. Phys Rev Lett, 1981, **46**: 953.
[33] SCHMIDT E, SCHRÖDER H, SONNTAG B, *et al*. J Phys B, 1984, **17**: 707.
[34] AKSELA S, SIVONEN J. Phys Rev A, 1982, **25**: 1243.
[35] HAAK H W, SAWATZKY G A, THOMAS T D. Phys Rev Lett, 1978, **41**: 1825.
[36] CASNATI E, TARTARI A, BARALDIT C, NAPOLI G. J Phys B, 1985, **18**: 2843.
[37] BERÉNYI D, HOCK G, RICZ S, *et al*. J Phys B, 1978, **11**: 709.
[38] JÖNSSON P, HE X, FROESE FISCHER C, *et al*. Comp Phys Commun, 2007, **177**: 597.
[39] FRITZSCHE S. Comp Phys Commun, 2012, **183**: 1525.
[40] GRANT I P, MCKENZIE B J, NORRINGTON P H, *et al*. Comp Phys Commun, 1980, **21**: 207.
[41] DYALL K G, GRANT I P, JOHNSON C T, *et al*. Comp Phys Commun, 1989, **55**: 425.
[42] GRANT I P. Relativistic Quantum Theory of Atoms and Molecules (New York: Springer), 2007.
[43] FANO U. Phys Rev, 1961, **124**: 1866.
[44] FANO U, COOPER J W. Phys Rev A, 1965, **137**: 1364.
[45] WAN J J, DONG C Z. Chin Phys B, 2009, **18**: 3819.
[46] ROOS B O, TAYLOR P R, SIEGBAHN P E M. Chemical Physics, 1980, **48**: 157.
[47] KRAMIDA A, RALCHENKO Yu, READER J, and NIST ASD Team (2015). NIST Atomic Spectra Database (ver. 5.3), [Online]. Available: http://physics.nist.gov/asd [2017, May 7]. National Institute of Standards and Technology, Gaithersburg, MD.

铜原子单激发态$3d^{10}4p\ ^2P_{1/2}$的光电离

顾素洁[1,2]，万建杰[1,†]，郭 娜[1]，马新文[2,†]

（1. 西北师范大学物理与电子工程学院，兰州 730070；
2. 中国科学院近代物理研究所，兰州 730000）

摘要： 铜原子能级结构的理论计算具有非常大的挑战性。本文基于多组态Dirac-Hartree-Fock(MCDHF)方法和相对论组态相互作用(RCI)方法，通过三个大规模的关联模型计算了单激发态$3d^{10}4p\ ^2P_{1/2}$、双激发态$3d^94s(^3D)5s\ ^4D_{3/2,1/2}$, $3d^94s(^3D)5s\ ^2D_{3/2}$, $3d^94s(^1D)5s\ ^2D_{3/2}$以及离子态$3d^{10}\ ^1S_0$能级和波函数。结果表明，铜原子能级结构对有限组态空间的选择极其敏感，双激发态$3d^94s(^3D)5s\ ^4D_{3/2,1/2}$, $3d^94s(^3D)5s\ ^2D_{3/2}$, $3d^94s(^1D)5s\ ^2D_{3/2}$和离子态$3d^{10}\ ^1S_0$与单激发态之间的能量差相对于已有实验结果均存在大约−0.4 eV的偏差，而计算得到的共振电子能量与实验结果符合得较好。此外，根据辐射跃迁矩阵元和非辐射跃迁矩阵元计算了双激发态的Fano参数q，并基于Fano理论得到了铜单激发态$3d^{10}4p\ ^2P_{1/2}$的总光电离截面，该理论考虑了直接光电离与光激发自电离之间的干涉效应，即共振$3d^94s(^3D)5s\ ^4D_{3/2,1/2}$ 、$3d^94s(^3D)5s\ ^2D_{3/2}$和$3d^94s(^1D)5s\ ^2D_{3/2}$具有明显的非对称的Fano轮廓，表明光电离过程与光激发自电离过程之间的干涉对双激发态共振附近的光电离截面轮廓有着极其重要的影响。

关键词： 多组态Dirac-Hartree-Fock(MCDHF)方法；单激发态；双激发态；铜原子；光电离截面

收稿日期： 2019-01-29； **修改日期：** 2019-02-26

基金项目： 国家自然科学基金资助项目(11320101003, 11204243)；西北师范大学物理与电子工程学院物理学科科研创新团队项目资助

† **通信作者：** 万建杰，E-mail: wanjj@nwnu.edu.cn；马新文，E-mail: x.ma@impcas.ac.cn。